Phonon dispersion relation in $LiKSO_4$

S. L. Chaplot, K. R. Rao, and A. P. Roy
Nuclear Physics Division, Bhabha Atomic Research Centre, Trombay, Bombay 400085, Maharashtra, India
(Received 1 July 1983; revised manuscript received 10 November 1983)

Extensive Raman scattering and neutron-diffraction studies of $LiKSO_4$ have recently been carried out in our laboratory at Trombay. In order to understand the experimental observations in Raman scattering, we have resorted to lattice-dynamical calculations. A model based on an atom-atom potential function comprised of the Coulombic and short-range interactions as well as covalent interactions is used to calculate the phonon dispersion relation in $LiKSO_4$ [in two space groups $P6_3$ (C_6^6) and $P31c$ (C_{3v}^4)]. The rigid molecular-ion model is used for studying external modes, and an atomic model is used for studying both the external and internal modes in the lattice. Comparison of the theoretical phonon frequencies with those obtained from optical techniques shows that for most of the frequencies the agreement is reasonable. From results of studies in which *one* of the parameters of the potential function was systematically varied, an incommensurate soft mode belonging to E_1^+ symmetry is predicted at a wave vector of nearly $0.4\vec{c}^*$. This mode involves librations of sulfate ion about axes in the basal plane. Details of analysis of phonon eigenvectors and LO-TO splittings are presented and compared with experimental results.

I. INTRODUCTION

The lattice modes in $LiKSO_4$ have been investigated by Raman scattering[1–4] and infrared absorption.[1] Physical properties such as thermal expansion[5] and dielectric constant[6,7] have also been studied, and several phase transitions have been suggested. It is believed that reorientation of the sulfate tetrahedra play an important role in these transformations. The vibrational energy levels of the sulfate ion in different crystalline environments are also of interest because of the distortion from the perfect tetrahedral configuration in the free state.[8,9]

In this paper we report a lattice dynamical study of $LiKSO_4$ in the room-temperature phase $P6_3$ (C_6^6) and in the low-temperature phase[2] $P31c$ (C_{3v}^4) ($T_c \sim 201$ K). These studies were undertaken to make the eigenvector assignments of the mode frequencies observed by Raman scattering and infrared absorption techniques as well as to compare the theoretical values of LO-TO splittings with those observed in infrared (ir) and Raman data.[1,2]

In Sec. II we recollect the crystallographic and group-theoretical information relevant to the dynamical problem of external and internal vibrations of $LiKSO_4$ in the solid state. This is followed, in Sec. III, by a description of the model of interatomic interactions used in this study. The adjustable parameters of the interaction potential function were arrived at by taking into account the equilibrium of the crystal. In this context, rotational invariance conditions have played a subtle role. Results of the calculations and discussion are given in Secs. IV and V, respectively.

II. CRYSTAL STRUCTURE AND GROUP-THEORETICAL CLASSIFICATION OF LATTICE VIBRATIONS

Crystal structure of $LiKSO_4$ at room temperature has been studied previously using x-ray diffraction[10] and recently by neutron diffraction.[11,12] At room temperature the system is associated with the space group $P6_3$ (C_6^6) (Ref. 13), and there are two molecules in the hexagonal unit cell as shown in Fig. 1. The cell dimensions and atomic coordinates obtained from neutron experiments are given in Table I. The atomic positions in the low-temperature phase $P31c$ (C_{3v}^4) have not been determined so far. For the purpose of our study, the atomic coordinates for this phase are obtained from the $P6_3$ phase on the basis of reorientation of the second sulfate tetrahedron (molecule number 6) by 60° in the $P31c$ phase as suggested in Ref. 2.

There is only one high-symmetry direction in the $P6_3$ phase and this is the hexagonal c axis (and corresponding-

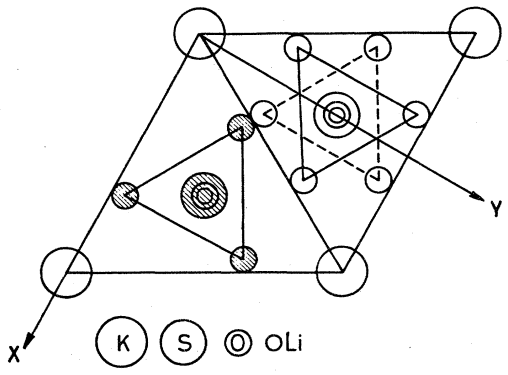

FIG. 1. Crystallographic structure of $LiKSO_4$. The figure shows projection on basal plane. Location of oxygens shown at the corners of the triangles, sides of which are in full lines, corresponds to the $P6_3$ phase. One of these tetrahedra is assumed to have rotated by 60° about the triad axis in the phase $P31c$, and oxygen positions in this phase are shown linked by dashed lines. Cartesian axes $\vec{x}$ and $\vec{y}$ are also shown. $\vec{z}$ axis is normal to the plane of the figure pointing outwards.

TABLE I. Atomic coordinates in phase $P6_3$ of $LiKSO_4$ at 300 K. $a=b=5.14$ Å, $c=8.617$ Å, $\alpha=\beta=90°$, and $\gamma=120°$.

Atom number	Atom	Molecule number	Fractional coordinates u	v	w
1	Li	1	$\frac{1}{3}$	$\frac{2}{3}$	0.8147
2	Li	2	$\frac{2}{3}$	$\frac{1}{3}$	0.3147
3	K	3	0	0	0
4	K	4	0	0	0.5
5	S	5	$\frac{1}{3}$	$\frac{2}{3}$	0.2066
6	O(1)		$\frac{1}{3}$	$\frac{2}{3}$	0.0357
7	O(2)		0.3417	0.9397	0.2587
8	O(2)		0.0603	0.4020	0.2587
9	O(2)		0.5980	0.6583	0.2587
10	S	6	$\frac{2}{3}$	$\frac{1}{3}$	0.7066
11	O(1)		$\frac{2}{3}$	$\frac{1}{3}$	0.5357
12	O(2)		0.6583	0.0603	0.7587
13	O(2)		0.9397	0.5980	0.7587
14	O(2)		0.4020	0.3417	0.7587

ly the $\vec{c}^*$ axis in reciprocal space). The modes propagating along the $\vec{c}^*$ direction can be classified in terms of the irreducible representations of the group of the wave vector $\vec{q}$, $G_0(\vec{q})$. The irreducible multiplier representations (IMR's) for the group of the wave vector, C_6 associated with the hexad axis are given in Table II(a). In the atomic model[14] appropriate to the study of both the external vibrations and the internal vibrations of the sulfates (SO_4^{2-}), there are 42 degrees of freedom associated with the unit cell. In the rigid molecular-ion model[15] where the sulfate ions are treated as rigid units, one is left with 24 degrees of freedom, associated with external modes only. The classification of the modes in terms of the IMR's are as follows: For the atomic model,

$$7A+7B+7E_1^+ +7E_1^- +7E_2^+ +7E_2^- .$$

For the rigid molecular-ion model,

TABLE II. Irreducible multiplier representations. (a) Phase $P6_3$ (C_6^6). In the space group $P6_3$, the operations C_6, C_2, and C_6^{-1} are associated with the fractional translation vector $\vec{\tau}=(0,0,\frac{1}{2})$. (b) Phase $P31c$ (C_{3v}^4). In the space group $P31c$, operations $\sigma_v(1)$, $\sigma_v(2)$, and $\sigma_v(3)$ are associated with the fractional translation vector $\vec{\tau}=(0,0,\frac{1}{2})$.

(a) Phase $P6_3$ (C_6^6); $\vec{q}$ along hexad axis; $G_0(\vec{q})=\{C_6\}$

	Point-group operations of C_6					
Representation	E	C_6	C_3	C_2	C_3^{-1}	C_6^{-1}
A	1	1	1	1	1	1
B	1	−1	1	−1	1	−1
E_1^+	1	ϵ	$-\epsilon^*$	−1	$-\epsilon$	ϵ^*
E_1^-	1	ϵ^*	$-\epsilon$	−1	$-\epsilon^*$	ϵ
E_2^+	1	$-\epsilon$	$-\epsilon^*$	1	$-\epsilon$	$-\epsilon^*$
E_2^-	1	$-\epsilon^*$	$-\epsilon$	1	$-\epsilon^*$	$-\epsilon$

$\epsilon=\exp(i\pi/3)$

(b) Phase $P31c$ (C_{3v}^4); $\vec{q}$ along the $\vec{c}^*$ axis; $G_0(\vec{q})=\{C_{3v}\}$

	Point-group operations of C_{3v}					
Representation	E	C_3	C_3^{-1}	$\sigma_v(1)$	$\sigma_v(2)$	$\sigma_v(3)$
A	1	1	1	1	1	1
B	1	1	1	−1	−1	−1
E	2	−1	−1	0	0	0

$$4A+4B+4E_1^+ +4E_1^- +4E_2^+ +4E_2^- \ .$$

The symmetry vectors for the modes propagating along the hexagonal axis and appropriate for the rigid molecular model were derived using standard group-theoretical techniques[14–16] and are given in Table III. These describe the nature of the "molecular" and atomic displacements corresponding to various representations and are also used for block diagonalization of the eigenvalue equations of the lattice motions in the numerical calculations.

An important point to note is that although the representations [in Table II(a)] are all one dimensional and, hence, degeneracy among modes belonging to the different IMR's is not demanded by spatial symmetry, additional degeneracy is expected due to time-reversal symmetry.[17] At the zone center, modes of E_1^+ symmetry should be degenerate with those of E_1^- and modes of E_2^+ with those of E_2^-. At the zone-boundary point $(0,0,\pm\frac{1}{2}c^*)$, the degenerate pairs are (E_1^+,E_2^-) and (E_1^-,E_2^+). In our study, we find that these demands of degeneracy due to symmetry lead to stringent constraints on the adjustable parameters of the potential.

The crystallographic structure of the low-temperature phase $P31c$ (C_{3v}^4) is also indicated in Fig. 1. The c axis continues to be the unique high-symmetry direction, now a triad axis, in this phase also. The IMR's of the point group C_{3v} underlying this space group are useful in classifying the modes propagating along the $\vec{c}^*$ axis and are given in Table II(b). The classification of modes in the atomic and rigid molecular-ion models for modes propagating along the $\vec{c}^*$ direction in this phase are as follows: For the atomic model,

$$7A+7B+14E \ .$$

For the rigid molecular-ion model,

$$4A+4B+8E \ .$$

Symmetry vectors of modes propagating along this direction in the $P31c$ phase are given in Table III for the rigid molecular-ion model.

III. INTERATOMIC INTERACTIONS

We assume that the S and O atoms within a sulfate cluster are covalently bonded and that different sulfate clusters and Li^+ and K^+ atoms interact via nonbonded interactions. We further assume that the latter interactions can be approximated by a sum of two-body atom-atom potentials given by

$$V(r_{kk'})=\frac{e^2}{4\pi\epsilon_0}\frac{Z(k)Z(k')}{r_{kk'}}+a\exp\left[\frac{-br_{kk'}}{R(k)+R(k')}\right] . \quad (1)$$

The first term is Coulombic in nature and the second is

TABLE III. Symmetry vectors for $LiKSO_4$ in rigid molecular-ion model for $\vec{q}$ along the $\vec{c}^*$ axis. x, y, and z refer to the translations along the x, y, and z axes. θ_x, θ_y, and θ_z refer to the librations about the x, y, and z axes. Numbers in parenthesis refer to the molecular numbers given in Table I. (a) Phase $P6_3$. (b) Phase $P31c$.

(a) Phase $P6_3$

Representation	Symmetry vectors
A	$z(1)+z(2)$, $z(3)+z(4)$, $z(5)+z(6)$, $\theta_z(5)+\theta_z(6)$
B	$z(1)-z(2)$, $z(3)-z(4)$, $z(5)-z(6)$, $\theta_z(5)-\theta_z(6)$
E_1^+	$x(1)+iy(1)+x(2)+iy(2)$, $x(3)+iy(3)+x(4)+iy(4)$, $x(5)+iy(5)+x(6)+iy(6)$, $\theta_x(5)+i\theta_y(5)+\theta_x(6)+i\theta_y(6)$
E_1^-	$x(1)-iy(1)+x(2)-iy(2)$, $x(3)-iy(3)+x(4)-iy(4)$, $x(5)-iy(5)+x(6)-iy(6)$, $\theta_x(5)-i\theta_y(5)+\theta_x(6)-i\theta_y(6)$
E_2^+	$x(1)+iy(1)-x(2)-iy(2)$, $x(3)+iy(3)-x(4)-iy(4)$, $x(5)+iy(5)-x(6)-iy(6)$, $\theta_x(5)+i\theta_y(5)-\theta_x(6)-i\theta_y(6)$
E_2^-	$x(1)-iy(1)-x(2)+iy(2)$, $x(3)-iy(3)-x(4)+iy(4)$, $x(5)-iy(5)-x(6)+iy(6)$, $\theta_x(5)-i\theta_y(5)-\theta_x(6)+i\theta_y(6)$

(b) Phase $P31c$

Representation	Symmetry vectors
A	$z(1)+z(2)$, $z(3)+z(4)$, $z(5)+z(6)$, $\theta_z(5)-\theta_z(6)$
B	$z(1)-z(2)$, $z(3)-z(4)$, $z(5)-z(6)$, $\theta_z(5)+\theta_z(6)$
E	$x(1)$, $x(2)$, $x(3)$, $x(4)$, $x(5)$, $\theta_x(5)$, $x(6)$, $\theta_x(6)$, $y(1)$, $y(2)$, $y(3)$, $y(4)$, $y(5)$, $\theta_y(5)$, $y(6)$, $\theta_y(6)$,

short-range repulsive. $r_{kk'}$ is the separation between atoms k and k'. The indices k and k' may refer to the ions Li^+ or K^+ or to any of the atoms that belong to *different* molecular units (sulfates). The coefficients a and b are assumed to be constants[18–20] with the values $a=1822$ eV and $b=12.364$. $Z(k)$ and $R(k)$, the charge and radius of atom k, are treated as parameters.

It is difficult to model the covalent-bond interaction in the sulfate clusters, as such an interaction should involve angle bending three-body interactions apart from the two-body bond stretching interactions. We have employed a simplified model in the present study by representing the S—O bond-stretching potential as[21]

$$V(r_{SO})=-cD\exp\left[-\frac{n}{2c}\frac{(r_{SO}-r_0)^2}{r_{SO}}\right], \quad (2)$$

with $c=1.0$, $n=15.2$ Å^{-1}, and $r_0=1.40$ Å. D is treated as a parameter. In order to simulate the potential of bending of O—S—O angles, we have assumed an O-O interaction for any two oxygen atoms of the same sulfate unit given by

$$V(r_{OO})=\frac{e^2}{4\pi\epsilon_0}\frac{[Z(O)]^2}{r_{OO}}+sa\exp\left[\frac{-br_{OO}}{2R(O)}\right]-\frac{w}{r_{OO}^6}, \quad (3)$$

where s and w are new parameters. Z(O) and R(O) are the charge and radius parameters, respectively, of the oxygen atoms that enter the nonbonded interaction given earlier by Eq. (1).

Naturally, the unknown parameters have to be chosen so as to obey the equilibrium conditions of the crystal structure.[22,23] The parameters $Z(k)$ and $R(k)$ in Eq. (1) are determined by the requirement of vanishing forces on the lithium and potassium atoms and the rigid sulfate clusters, and vanishing torques on sulfates when the forces and torques are evaluated at their equilibrium positions and orientations. In addition, it is ensured that the parameters yield a reasonable value for the cohesive energy of the crystal as expected from the known cohesive energies of other ionic crystals.

IV. RESULTS

We have carried out calculations based on the rigid molecular-ion model[15] and the atomic model[14] to examine the nature of lattice modes and to comment on various aspects of Raman and ir data in both the phases $P6_3$ and $P31c$. Phonon dispersion curves along the $\vec{c}^*$ and $\vec{a}^*$ axes have been obtained. Effect of variation of some of the potential parameters on these curves have revealed certain new features of softening that would be of interest to experimentalists. We shall first discuss details of the phonon dispersion curves and then comment specifically on aspects related to Raman and ir data.

The program DISPR (Ref. 24) was used to compute lattice frequencies in the rigid molecular-ion model. The program was suitably modified to take into account covalent bond interactions in the atomic model calculations. The input parameters are the structural data given in Table I and the symmetry vectors[25] given in Table III in addition to the potential parameters.

The potential parameters of Eq. (1) were obtained by making use of the equilibrium conditions[22,23] and also some of the Raman frequencies. Least-squares fitting with Raman frequencies was, however, not attempted. The charges $Z(k)$ and $R(k)$ of the atoms Li, K, S, and O are 0.95, 0.55, 1.1, and −0.65 and 1.375, 1.95, 1.0, and 1.35 Å, respectively. We find that equilibrium conditions had to be satisfied exactly to ensure degeneracy of the modes at zone center.

A. Rigid molecular-ion model (external modes only)

1. Phase $P6_3$

Phonon dispersion curves calculated along the c^* axis and the a^* axis are given in Figs. 2(a) and 3, respectively. We note that the frequencies at zone center are in reasonable agreement with those obtained from Raman and ir data, as will be discussed later in Sec. V. But more importantly, we wish to draw attention to a striking feature that can be seen in Fig. 2(a), namely, the occurrence of a dip in the transverse acoustic branch of E_1^+ symmetry. There is an anticrossing between this TA branch with another TO branch of the same symmetry, and thus the soft mode associated with the dip should be considered as a TO mode. The mode is found to be highly sensitive to the short-range potential parameters R(Li) and R(O). The variation of the low-frequency phonon branches with R(Li) is shown in Fig. 4(a). The small variation in R(Li), however, does not affect significantly the static equilibrium, but if R(O) is varied, then R(K) also has to be varied to maintain equilibrium. Since the softening of the branch occurs at nearly $0.4\vec{c}^*$, it can lead to an incommensurate phase transition. The eigenvector of the soft mode involves mainly libration of sulfate ions about axes in the basal plane. In order to predict the thermodynamic parameters at which the incommensurate phase transition may be observed, it is necessary to calculate the free energy of the system as a function of the thermodynamic parameters and locate its minimum.[26]

Results discussed so far have certain similarities to those in the study of K_2SeO_4 in which an incommensurate soft transverse-optic mode was observed[27] by inelastic neutron scattering. Subsequently lattice-dynamical calculations[28] have sought to understand the nature of this soft-mode behavior. The nature of bonding in K_2SeO_4 is expected to be generally similar to that in $LiKSO_4$ although crystallographic structures of the two systems are quite different. In the dynamical calculations of K_2SeO_4 (Ref. 28) employing the rigid-ion model the soft mode was "simulated" by small variations in a few of the force-constant parameters. However, the atomic displacements, associated with the soft mode in K_2SeO_4 derived theoretically, do not agree well[28] with those derived from the experiment, and this disagreement is attributed to certain effects of anharmonicity due to mode couplings on the experimental determination of these displacements as well as to the simplicity of the rigid-ion model that is employed. In this respect it would be interesting to verify experimentally the existence of a soft mode and determine its eigenvector in $LiKSO_4$ also.

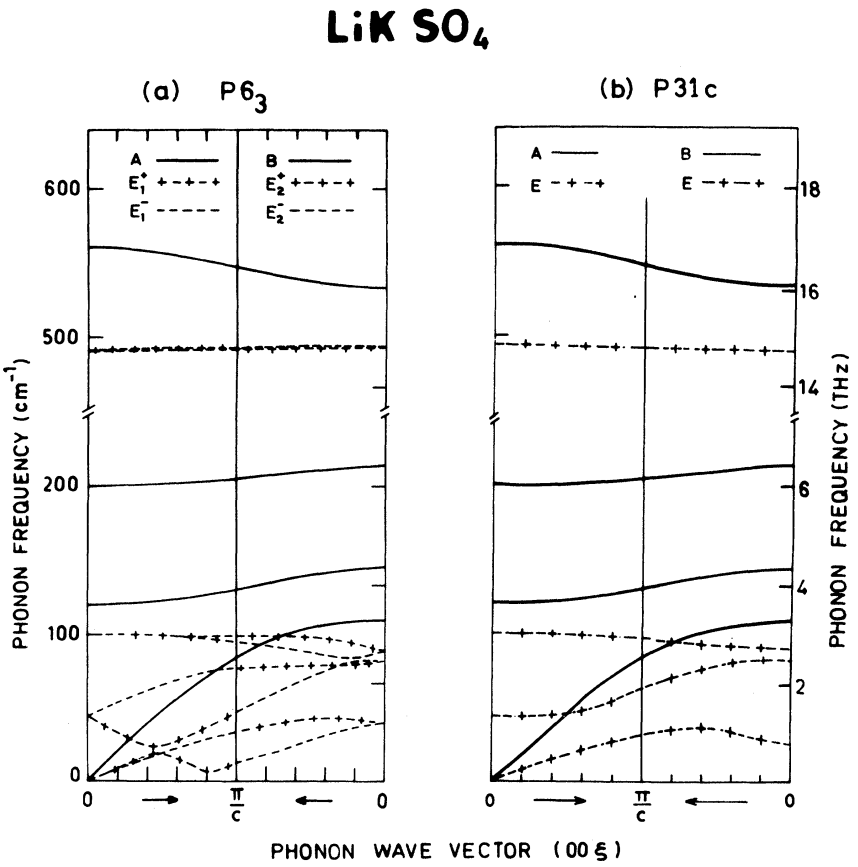

FIG. 2. (a) Phonon dispersion curves of $LiKSO_4$ in the phase $P6_3$ along the hexad axis. (b) Phonon dispersion curves in $LiKSO_4$ in the phase $P31c$ along the $\vec{c}^*$ axis. Both the figures are drawn in extended-zone scheme.

The dispersion curves in the basal plane of $LiKSO_4$ belong to a single representation because the group of the wave vector for any wave vector in this plane contains only one element, namely the identity operation. Anticrossing of various branches in any direction in the basal plane arises because of this feature. Figure 3 shows the nature of dispersion curves along the $\vec{a}^*$ direction. No softening of phonon branches occurs along this direction.

2. *Phase P31c*

The external mode frequencies for this phase were calculated with the same set of parameters as was used for the phase $P6_3$, but making use of appropriate crystal structure information and symmetry vectors for this phase. It may be noted that there are two one-dimensional representations and one two-dimensional representation associated with the point group C_{3v}, the group of the wave vector for $\vec{q}$ along the $\vec{c}^*$ axis. Consequently, in this phase we have some modes (those belonging to E representation) doubly degenerate due to spatial symmetry along this direction. In addition, at the zone boundary along $\vec{c}^*$, the A and B modes are degenerate and the E modes are fourfold degenerate due to time-reversal symmetry.

Phonon dispersion curves for this phase along the $\vec{c}^*$ axis are shown in Fig. 2(b). In comparison with the curves for the $P6_3$ phase shown in Fig. 2(a), we note that

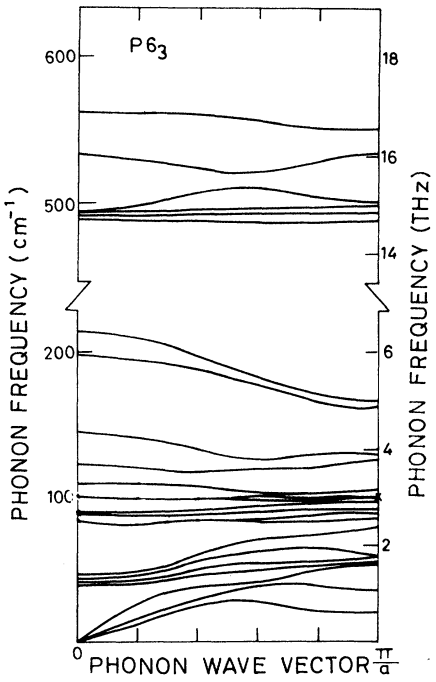

FIG. 3. Phonon dispersion curves of $LiKSO_4$ in the phase $P6_3$ along the $\vec{a}^*$ axis in the basal plane. The figure is drawn in reduced-zone scheme.

the A- and B-type modes are similar in both the phases. Secondly, at zone center and zone boundary, the E-type modes in phase $P31c$ have approximately the same frequencies as those of the E_1^+, E_1^-, E_2^+, and E_2^- modes in phase $P6_3$. These observations are borne out experimentally in that the frequencies do not change appreciably at $\vec{q} \sim \vec{0}$ in going from $P6_3$ to $P31c$ (except for the E_1 mode at 41 cm^{-1}). But one observes differences in behavior inside the Brillouin zone, that is, in the range of $0 < q < \pi/c$, as the E modes are doubly degenerate throughout this range. Alternate branches of the E-type modes in the $P31c$ phase are shown in the left- and right-hand sides of Fig. 2(b) only to help in comparison with the curves of phase $P6_3$.

Figure 4(b) shows the low-frequency branches as a function of variation of the parameter R(Li). Unlike in the case of phase $P6_3$, there is no softening that can lead to an incommensurate phase.

B. Atomic model calculations (external and internal modes)

The atomic model allows inclusion of all the internal modes also. As mentioned in Sec. II, the potentials are given by Eqs. (1)—(3). The calculations were restricted to phase $P6_3$ only, and dispersion curves were derived for wave vectors along the $\vec{c}^*$ and $\vec{a}^*$ axes. In conjunction with Eq. (1), the same values of parameters, as in external mode calculations, were used. As far as Eqs. (2) and (3) are concerned, two sets of calculations were carried out with the parameters D, s, and w given by 5.3 eV and 1 and 15 eV Å^6, respectively, in one set and another in which they were 3.6 eV and 70 and 780 eV Å^6. The first set of values were chosen on the basis that the frequencies of the internal modes ν_3 and that of the external modes are similar to those from the experiments but the frequencies of angle-bending vibrations may not be properly reproduced. The second set of the covalent parameters were derived by using the internal frequency ν_4, corresponding to O—S—O angle-bending vibration. Results of both calculations are given in Table IV. Atomic model calculations for phase $P31c$ were not carried out as rather little additional information can be obtained.

V. DISCUSSION

A. Comparison with optical data in phase $P6_3$

Comparison of calculated and experimental frequencies at $\vec{q} \sim \vec{0}$ can be made from Table IV. Group-theoretical labeling of modes in the experiments was obtained by carrying out experiments in different configurations of the crystal with respect to the incident and scattered light beams and their polarizations. From Table IV we make the following observations.

(i) The experimentally measured frequencies fall into nearly three distinct ranges: (a) 1200—1000 cm^{-1}, comprising the ν_3 and ν_1 internal modes; (b) 650—370 cm^{-1}, comprising the ν_4 and ν_2 internal modes and some external modes, a mixed region; and (c) 200—0 cm^{-1}, comprising the purely external modes.

(ii) Results of rigid molecular-ion and the atomic model calculations also show the three distinct categorization of frequencies given in (i) above.

(iii) Results of rigid molecular-ion model calculations indicate that agreement between calculated and observed mode frequencies up to 200 cm^{-1} is within about 50

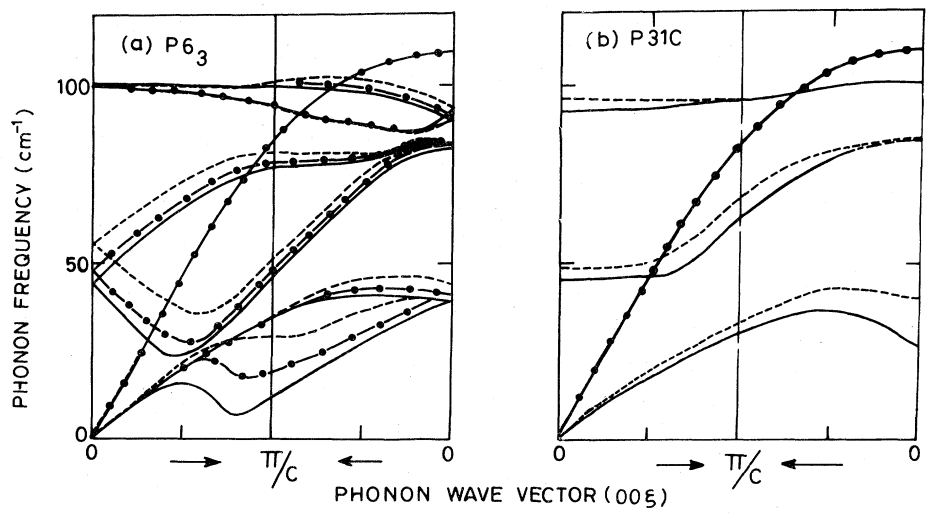

FIG. 4. (a) Low-frequency modes in phase $P6_3$ along the hexad axis as a function of variation of the parameter R(Li). The values of R(Li) corresponding to the dashed line, chain line, and solid line are 1.36, 1.37, and 1.375, respectively. (b) Low-frequency modes in phase $P31c$ along the $\vec{c}^*$ axis as a function of variation of the parameter R(Li). The values of R(Li) corresponding to the dashed line and solid line are 1.36 and 1.375, respectively. Both figures are drawn in extended-zone scheme. Modes of A and B representation do not show any variation.

TABLE IV. Comparison of experimental and calculated lattice frequencies at zone center.

Representation[a]	Internal modes[b]	Experimental values[c] (cm^{-1})	Calculated values (cm^{-1}) $P6_3$ phase: Atomic model[d]	$P6_3$ phase: Atomic model[e]	$P6_3$ phase: Rigid molecular-ion model	$P31c$ phase: Rigid molecular-ion model
A	ν_3	1201	1180	1367		
		1122	1161	1367		
	ν_1	1012	967	1138		
		1012	967	1128		
	ν_4	630	547	608		
		624	492	547		
		430	331	521	561	561
		370	277	482	490	490
		204	224	207	200	200
		202	221	204	197	197
		162	116	119	121	120
		131	100	101	101	101
			acoustic	acoustic	acoustic	acoustic
B	ν_3		1174	1367		
	ν_1		971	1136		
	ν_4		561	627		
			277	475	534	534
			224	218	213	214
			138	142	144	145
			110	109	109	109
E_1^+, E_1^-	ν_3	1200	1216	1159		
		1119	1199	1150		
	ν_4	649	576	650		
		636	508	600		
	ν_2	445	320	596		
		466	289	577		
		478	218	496	563	563
		408	217	466	491	491
		164	128	122	123	124
		133	126	100	100	100
		44	117	52	46	
		41	99	50	44	27
			acoustic	acoustic	acoustic	acoustic
E_2^+, E_2^-	ν_3	1123	1199	1150		
	ν_4	637	512	601		
	ν_2	467	292	576		
		404	197	465	493	493
		131	139	92	89	91
			82	83	82	84
			61	42	39	45

[a]The modes of E type in the $P31c$ phase are distributed under the E_1 and E_2 representations to show that the frequencies remain almost unaltered in going from $P6_3$ phase to $P31c$ phase, except the E_1^+, E_1^- modes in the $P6_3$ phase at 44 cm^{-1}.

[b]ν_1, ν_2, ν_3, and ν_4 are internal modes of the sulfate ion.

[c]The pairs of frequencies shown together by a curly bracket are LO-TO counterparts of a mode with respect to the wave vector along the $\bar{c}^*$ axis.

[d]$D=5.3$ eV, $s=1$, and $w=15$ eV Å^6.

[e]$D=3.6$ eV, $s=70$, and $w=780$ eV Å^6.

cm^{-1}. The agreement is rather poor in the mixed region of frequencies. The atomic model results do not significantly differ from those of the rigid molecular-ion model in the purely external mode region except for a set of frequencies at 117 cm^{-1} and 99 cm^{-1} of the E_1 representation in one of the atomic model calculations.

(iv) The highest frequencies of the A representation are well reproduced in the atomic model calculations with $D=5.3$ eV, $s=1$, and $w=15$ eV Å^6. These vibrations essentially involve S—O stretching and therefore are deter-

mined by the potential given in Eq. (2). However, in the mixed region of frequencies, agreement between results of this atomic model calculation and experiments is rather poor. In the second calculation based on the atomic model, with the parameters $D=3.6$ eV, $s=70$, and $w=780$ eV Å^6, agreement in the mixed range of frequencies improves as one would expect. But now the nature of LO-TO splittings in the mixed and highest-frequency ranges are grossly distorted.

These observations lead us to believe that the rigid molecular-ion model gives a fairly good representation of modes in the purely external mode region (see further discussion on LO-TO splittings in this region). The atomic model description has to be modeled in a different way to take into account the angle bending and bond stretching, etc., in a more natural way, say, by a valence force model. Results from the atomic model calculations would yield better agreement in the mixed region of frequencies if one makes allowance for electronic polarization or three-body interactions. We have not persued these options any further since our objective was limited to understanding the nature of modes observed experimentally; this objective is met even with the limited studies reported in this paper by examining the nature of eigenvectors, LO-TO splittings, and the effect of variation of parameters on the calculated lattice frequencies. We shall discuss these aspects now.

TABLE V. Square of the component of mass-weighted eigenvector $|\vec{e}^{\,i}_j(k)|^2$ for the external modes at (a) $\vec{q}=0.002\vec{c}^{\,*}$ and (b) $\vec{q}=0.5\vec{c}^{\,*}$. $i=T$ (translation) or R (rotation) of various vibrating units; j=mode index and k=molecular index.

j	Representation	Calculated frequency (cm^{-1})	$\lvert\vec{e}^{\,i}_j(k)\rvert^2$ T(Li)	T(K)	$T(SO_4^{2-})$	$R(SO_4^{2-})$
			(a) $\vec{q}=0.002\vec{c}^{\,*}$			
1	A	acoustic	0.05	0.27	0.68	0.00
2		121	0.04	0.72	0.23	0.01
3		200	0.00	0.01	0.01	0.98
4		561	0.91	0.00	0.08	0.01
5	B	109	0.00	0.97	0.01	0.02
6		144	0.01	0.03	0.73	0.23
7		213	0.00	0.00	0.26	0.74
8		534	0.99	0.00	0.00	0.01
9	E_1^+, E_1^-	acoustic	0.05	0.27	0.68	0.00
10		44	0.01	0.00	0.00	0.99
11		100	0.01	0.73	0.26	0.00
12		491	0.93	0.00	0.06	0.01
13	E_2^+, E_2^-	39	0.04	0.03	0.46	0.47
14		82	0.01	0.71	0.19	0.09
15		89	0.01	0.26	0.30	0.43
16		493	0.94	0.00	0.05	0.01
			(b) $\vec{q}=0.5\vec{c}^{\,*}$			
1	A, B	84	0.01	0.58	0.39	0.02
2		131	0.04	0.41	0.49	0.06
3		205	0.00	0.01	0.08	0.91
4		548	0.95	0.00	0.04	0.01
5	E_1^+, E_2^-	12	0.02	0.07	0.14	0.77
6		47	0.03	0.20	0.55	0.22
7		95	0.02	0.74	0.24	0.00
8		493	0.93	0.00	0.06	0.01
9	E_1^-, E_2^+	33	0.05	0.18	0.65	0.12
10		77	0.00	0.31	0.02	0.67
11		99	0.02	0.50	0.28	0.20
12		492	0.93	0.00	0.06	0.01

B. Eigenvector assignment

Table V provides the square of the component of mass-weighted eigenvectors $|\vec{e}_j^{\,i}(k)|^2$ corresponding to the translation and rotation of an atomic or molecular unit k for all the external modes at zone center ($\vec{q}=0.002\vec{c}^{\,*}$) and zone boundary ($\vec{q}=0.5\vec{c}^{\,*}$) This information along with the symmetry-vector information given in Table III has been useful in arriving at the nature of dynamics associated with the various Raman and ir frequencies. The present calculations have also provided definite information about libration frequencies of the sulfate ions in $LiKSO_4$. An interesting feature that emerges is that the frequency corresponding to libration of SO_4^{2-} at zone center about the c axis (A mode at 200 cm^{-1}) is widely different from that about an axis perpendicular to this axis (E_1^+, E_1^- mode at 44 cm^{-1}). Detailed examination of the eigenvectors of these modes from Table V(a) shows that mixing of these rotational modes with any other translational mode is negligible. Experimentally, although both the modes have been observed, only the A mode could be identified with librations using the combined ir and Raman data. The other significant result is that along the c^* axis throughout the Brillouin zone these modes are predominantly rotational in character. This feature is likely to be independent of specific choice of potential parameters employed in the present calculation. The fact that the $E_1(E_1^+, E_1^-)$ mode corresponding to librations about axes in the basal plane is rather soft could reflect in large amplitude of such motions. Recent analysis of the structural data by neutron diffraction[12] corroborates this picture in the sense that the displacement of the O(1) atom perpendicular to the S—O(1) bond is significantly large, suggesting comparatively less hindrance to such libratory motion.

C. LO-TO splittings in the $P6_3$ phase

We now wish to comment on the nature of LO-TO splittings of various modes ($\vec{q}\sim\vec{0}$). The modes belonging to the A and E_1 (E_1^+ and E_1^-) representations only are polar and therefore they only exhibit LO-TO splittings. Examination of the symmetry vectors (given in Table III) shows that the LO modes belong to the A and B representation and the TO modes to the E_1 and E_2 representations, with respect to the wave vector $\vec{q}$ along the $\vec{c}^{\,*}$ axis.[29] In order to comment on the LO-TO splittings, we have to identify the TO modes that belong to the A-type representation and LO modes of the E_1-type representation. These will be modes associated with the wave vectors in the basal plane. However, since the group of the wave vector for waves in the basal plane contains the identity operation only, all the modes belong to a single representation, strictly speaking. In spite of this situation we have followed the scheme given below in order to classify modes. From among the modes that propagate in the basal plane, first we collect those TO modes having atomic displacements along the z axis. One set of modes among these has frequencies very close to those of the B modes propagating along the $\vec{c}^{\,*}$ axis. The remaining modes of this TO category are labeled as TO modes of the A representation. Next we collect modes having displacement in the basal plane. Once again there is one set with frequencies nearly identical to those of E_2 modes propagating along the $\vec{c}^{\,*}$ axis and they are doubly degenerate. The remaining two sets (one set of TO modes and another of LO modes) are labeled as modes of E_1 representation. In fact we find that the difference between modes of either B or E_2 representations for wave vectors $\vec{q}\sim 0$ along the $\vec{c}^{\,*}$ and $\vec{a}^{\,*}$ axes are less than 1 cm^{-1} and hence we believe that our procedure of labeling is reasonable.

In Table VI we give a comparison of the LO-TO splittings of the external modes at zone center as measured experimentally and as calculated using the rigid molecular-ion model and the atomic model. Although the absolute values of the frequencies may not match, particularly in the intermediate region of frequencies for reasons already discussed, the splittings as observed in the experiments are in good agreement with the theoretical calculations.

VI. SUMMARY

We have reported in this paper the results of a lattice dynamical calculation of the lattice frequencies of the complex crystal $LiKSO_4$ based on an atomic model and the rigid molecular-ion model. The nature of atom-atom potentials used include parametrized Coulomb and short-range interactions as well as covalent-bond interactions. The rigid molecular-ion model using Coulombic and short-range interactions provides a reasonable explanation

TABLE VI. Comparison of LO-TO splittings at zone center for the external modes on the basis of rigid molecular-ion model in the $P6_3$ phase. Δ=LO-TO.

	Experimentally observed frequencies (cm^{-1})			Calculated frequencies (cm^{-1})					
				Rigid molecular-ion model			Atomic model		
Representation	LO	TO	Δ	LO	TO	Δ	LO	TO	Δ
A	430	370	60	561	490	71	521	482	39
	204	202	2	200	197	3	207	204	3
	162	131	31	121	101	20	119	101	18
E_1^+, E_1^-	478	404	74	563	492	71	496	466	30
	164	133	31	123	100	23	122	100	22
	44	41	3	46	44	2	52	51	1

of the observed Raman and infrared data in the external mode region where effects of internal vibrations are not expected to be felt. Inclusion of covalent interactions in the sulfate ion explains the bond-stretching high-frequency modes.

These calculations have provided the correct assignments of the Raman and ir data in the phases $P6_3$ and $P31c$ and have helped in understanding the nature of various modes observed. The nature of LO-TO splittings observed experimentally is borne out by the rigid molecular-ion model calculations providing additional support to the model.

The phonon dispersion curves would be helpful in comparing with the neutron data as and when they become available. An interesting outcome of the calculations is the observation of a soft mode that leads us to predict that there may be an incommensurate phase transition corresponding to a soft mode at around $0.4\vec{c}^*$ (or $0.8\pi/c$) from the $P6_3$ phase and this mode involves librations of sulfate ions. It remains to be investigated under what thermodynamic conditions such a softening would be observable experimentally.[30] Inelastic neutron experiments as a function of temperature or pressure may throw some light on this aspect and help in developing better theoretical models.

[1]J. Hiraishi, N. Taniguechi, and H. Takahashi, J. Chem. Phys. 65, 3821 (1976).

[2]M. L. Bansal, S. K. Deb, A. P. Roy, and V. C. Sahni, Solid State Commun. 36, 1047 (1980).

[3]M. L. Bansal, S. K. Deb, A. P. Roy, and V. C. Sahni, Pramana 20, 183 (1983).

[4]D. Teeters and R. Frech, Phys. Rev. B 26, 5897 (1982).

[5]D. P. Sharma, Pramana 13, 223 (1979).

[6]R. Ando, J. Phys. Soc. Jpn. 17, 937 (1962).

[7]T. Breczewski, T. Krajewski and B. Mroz, Ferroelectrics 33, 9 (1981).

[8]G. J. Wu and R. Frech, J. Chem. Phys. 66, 1352 (1977).

[9]M. L. Bansal, S. K. Deb, A. P. Roy, and V. C. Sahni, J. Phys. (Paris) 42, C6-902 (1981).

[10]A. Bradley, Philos. Mag. 49, 1225 (1925); M. Karppinen, J. O. Lundgren, and R. Liminga, Acta Crystallogr. Sect. C 39, 34 (1983).

[11]S. Bhakay Tamhane, A. Sequeira, and R. Chidambaram, Acta Crystallogr. Suppl. A37, C108 (1981).

[12]A. Sequeira (private communication).

[13]Recent structure work (Ref. 12) indicates that although the crystal displays pseudohexagonal symmetry, the correct space group is $P2_1$. Phonon frequency measurements by Raman scattering (Ref. 2), however, do not reveal any departure from the hexagonal symmetry, and consequently we shall adopt the space group $P6_3$ in our discussion.

[14]A. A. Maradudin and S. H. Vosko, Rev. Mod. Phys. 40, 1 (1968).

[15]G. Venkataraman and V. C. Sahni, Rev. Mod. Phys. 42, 409 (1970).

[16]M. Sieskind, J. Phys. Chem. Solids 39, 1251 (1978).

[17]M. Lax, *Symmetry Principles in Solid State and Molecular Physics* (Wiley, New York, 1974).

[18]K. R. Rao, S. L. Chaplot, P. K. Iyengar, A. H. Venkatesh, and P. R. Vijayaraghavan, Pramana 11, 251 (1978).

[19]S. L. Chaplot and K. R. Rao, J. Phys. C 13, 747 (1980); 16, 3045 (1983).

[20]S. L. Chaplot and V. C. Sahni, Phys. Status Solidi B 96, 575 (1979).

[21]E. R. Lippincott and R. Shroeder, Acta. Crystallogr. 23, 1131 (1955).

[22]S. L. Chaplot, V. C. Sahni, and K. R. Rao, Phys. Status Solidi 95, K99 (1979).

[23]S. L. Chaplot, V. C. Sahni and K. R. Rao, Acta Crystallogr. Sect. A 37, 374 (1981).

[24]S. L. Chaplot, Bhabha Atomic Research Centre Report No. BARC-972, 1978 (unpublished).

[25]The symmetry vector matrix is complex. For block-diagonalization purposes, we derived a real symmetry-vector matrix by taking linear combination of symmetry vectors belonging to the IMR's E_1^+ and E_1^- together and similarly those belonging to E_2^+ and E_2^- representations. Therefore group-theoretical information was used to block diagonalize the dynamical matrix into A, B, E_1 (block size of 14×14 in the rigid molecular-ion model comprised of $7E_1^+$ and $7E_1^-$ modes; the superscript is dropped for this reason) and E_2 blocks only. Further diagonalization was carried out by brute force numerical procedures.

[26]L. L. Boyer and J. R. Hardy, Phys. Rev. B 24, 2577 (1981).

[27]M. Iizumi, J. D. Axe, G. Shirane, and K. Shimaoka, Phys. Rev. B 15, 4392 (1977).

[28]M. S. Haque and J. R. Hardy, Phys. Rev. B 21, 245 (1980).

[29]This is not so for a few of the symmetry vectors. However, we note that the librations belonging to the A representation are not polar and the librations belonging to the E_1 representations aquire slight polarity due to the small distortion of the sulfates from the tetrahedral geometry.

[30]C. M. A. Fonseca, G. M. Ribeiro, R. Gazinelli, and A. S. Chaves, Solid State Commun. 46, 221 (1983). These authors have suggested the possibility of incommensurate phase transitions in $LiKSO_4$ at low temperatures based on their EPR work.